Bias-Free Predictive Control of Power Converters with LCL-Filter in Micro-Energy Systems

Xing, Qianli; Zhang, Zhenbin; Dragicevic, Tomislav; Rodriguez, Jose

Published in:
IEEE Transactions on Industrial Electronics

Link to article, DOI:
10.1109/TIE.2022.3196360

Publication date:
2023

Document Version
Peer reviewed version

Bias-Free Predictive Control of Power Converters with LCL-Filter in Micro-Energy Systems

Qianli Xing, *Student Member, IEEE*, Zhenbin Zhang*, *Senior Member, IEEE*, Tomislav Dragičević, *Senior Member, IEEE*, and Jose Rodriguez, *Life Fellow, IEEE*

***Abstract*—Power converters with LCL filters have been widely adopted in, e.g., micro-energy systems (MES), grid-tied renewable energy systems, etc. Such a system forms a high-order *multiple input and multiple output* (MIMO) dynamic system, requiring complicated active damping and showing slow control dynamics, applying classical cascaded linear controllers. Model predictive control (MPC) is a powerful control strategy which inherently suits for MIMO systems with constraints. However, for such systems, inevitable tracking biases are seen when using the classical MPC. Additionally, the nonlinear nature of the underlying system leads to difficulty for a deep analysis of an MPC controller design. In this work, we mathematically reveal the cause of tracking biases when applying classical MPC and develop an equivalent modeling method to eliminate it at both parameter and model uncertainties, forming a *robust and bias-free MPC*. The proposed solution remains fast in control dynamics and simple in structure. *Both* simulation *and* experimental data confirm the effectiveness of the proposed solution in mitigating tracking bias, and good robustness at model deviations and grid disturbances.**

***Index Terms*—Bias-free predictive control, LCL-filtered power converters, equivalent modeling method, high order nonlinear control dynamics, MIMO, micro-energy systems**

I. Introduction

REALIZATION of carbon neutrality policy largely depends on the development of renewable energy technologies. Grid-tied power converters (as shown in Fig. 1) play a critical role in renewable energy applications, which are widely used in, e.g., micro-energy systems (MES) [1], distributed power generation systems (DPGSs), energy storage systems, AC/DC micro-grids, etc.

The LCL-filtered converter is a cost-effective topology for the grid-tied power converters, due to its good high-frequency harmonic restraint capability, smaller size, and lower cost than a simple L- or LC-filter at large power ratings [2].

This work was supported in part by the National Distinguished Expert (Youth Talent) Program of China under Grant 31390089963058; in part by the General Program of National Natural Science Foundation of China under Grant 51977124; in part by the Natural Science Foundation of Jiangsu Province under Grant BK20190204; in part by the Several Policies on Promoting Collaborative Innovation and Achievement Industrialization of Universities and Research Institutes (Trial) under Grant 2020GXRC009; and in part by the Shenzhen Fundamental Research Program under Grant JCYJ20210324132616040. J. Rodriguez acknowledges the support of ANID through projects FB0008, 1210208 and 1221293. Zhenbin Zhang is the corresponding author, email: zbz@sdu.edu.cn.

Qianli Xing and Zhenbin Zhang are with the Lab. for More Power Electronics Energy Systems (MPEES), School of Electrical Engineering, Shandong University, Jinan 250061, China (e-mail: qianli.xing@mail.sdu.edu.cn; zbz@sdu.edu.cn).

Tomislav Dragičević is with the Electrical Engineering Department, Technical University of Denmark, 2800 Copenhagen, Denmark (e-mail: tomdr@dtu.dk).

J. Rodriguez is with Facultad de Ingenieria, Universidad Andres Bello, Santiago 8370146, Chile (e-mail: jose.rodriguez@unab.cl).

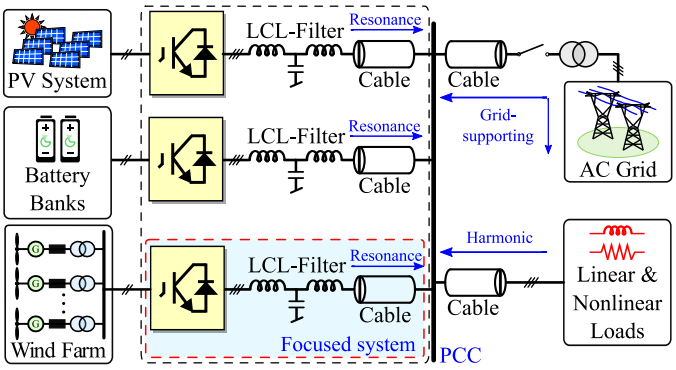

Fig. 1: Schematic diagram of LCL-filtered grid-tied converters-Based MES.

However, as a three-order system, the LCL-filters are easy to cause oscillation and resonance [3]. Hence they require appropriate damping techniques, i.e., passive damping (PD) or active damping (AD), to work properly, which leads to a complex control problem. PD inserts a resistor or resistors to dampen the resonance, causing high power losses for large power conversion systems. AD directly modifies the exiting controller, without additional resistors, which is therefore preferred in high-power converter system applications [4].

Control objectives of the underlying multiple input and multiple output (MIMO) system (shown in Fig. 1) include (at least) [5]: (i) resonance restraint; (ii) precise current/power tracking performance; and (iii) robustness to model and parameter deviations and grid disturbances. To cope with the aforementioned control objectives, when applying the classical cascaded PI based control solutions, a complex design process and low control dynamics are inevitably seen.

With the development of modern digital control platforms, model predictive control (MPC) has become a powerful alternative for power converters since two decades. Compared with classical voltage-oriented control or direct power control strategies, MPC is inherently suitable for MIMO systems by using a straightforward cost function design, and is able to include system nonlinearities and constraints. Remarkably, as one of the dominating branches of MPC, the finite-control-set MPC (FCS-MPC) combines the discrete-switching position selection with the optimization processes into a single step, requiring no time-averaged modulation, which offers the potential to reduce switching losses at good power quality [6], [7]. Besides, for the underlying system, extra merit is that predictive control achieves system stability and effectively balances uncontrolled resonant energy between the inductors and capacitance, without additional active damping methods.

However, existing predictive methods for the LCL-filtered converter have two key issues, i.e., (a) steady state tracking bias, the inner state (i.e., filter capacitor voltage and converter

side inductance current) reference cumulative error (in high-order system led by discretization process) will cause tracking bias when FCS-MPC is applied, which cannot be modeled by linear analysis tool. Besides, the grid voltage will directly influence the output current (See Eq. (9), the former is a direct feed-through item to the latter). (b) Imprecise equalization of FCS-MPC due to irregular discrete switching nature of FCS-MPC and unconsidered disturbances. Classical FCS-MPC usually deals only with the inner (power or current) control. An outer control loop to generate parts of the references[1], is therefore further needed, design of which requires a rough linearization approximating process, applying only for a very narrow range near the operating points, but hardly considers the undesirable disturbances and model deviations. The above issues motivate numerous research.

For issue (a), researchers present some solutions, which can be classified into two major types: feed-forward compensation and closed-loop compensation. The authors in [8]–[11] presented partial (e.g., [8], [9]) and full (e.g., [10], [11]) grid-disturbance feed-forward based techniques to eliminate the grid voltage disturbances, through an tunable equivalent impedance to grid harmonics. Taking inner state-variable and grid voltage as a feed-forward item, the solution is effective in dealing with the discrete cumulative error at reference generation process. However, an additional modulator will complicate system structure when using FCS-MPC. Authors of [12], [13] proposed an interesting method with FCS-MPC based techniques to address parts of issue (a). It successfully indicated that a proper designed closed-loop method combined with MPC works well without tracking bias. However, it lacks the proper theory to quantitatively analyze and unit the linear and nonlinear control design parts in underlying system .

To tackle the aforementioned problem (b), authors in [11] proposed a modulated-based MPC method to quantitatively analyze the controller performance by linear analysis tool. In [12], [14], offline describing function methods were used to describe underlying system's open-loop frequency response with FCS-MPC control, which lends linear analysis tools to assess the control scheme performance. However, both proposals show inflexibility and imprecision in running the underlying system at large operation range and parameter variations situations, aside with considerably increased efforts due to complexity of the controller design. Besides, artificial-intelligence-based (AI-based) methods provide an alternative solution [15], which is proper to control or model complex plants and systems with unclear topologies. While classical explicit modeling based techniques are more suitable for systems with clear and relatively simple structures and matured design and analysis tools [16], [17]. Despite its prospects, AI-based techniques are outside the scope of this work.

In this work, we propose an enhanced bias-free predictive control for the LCL-filtered grid-tied converters in MES. Different from the aforementioned works, we divide the causes for tracking bias into a *describable part* (caused by, e.g., grid disturbances) and *implicit part* (caused by, e.g., disturbances and inner reference state cumulative error). On this base, we establish a mathematical model to describe the underlying system[2]. Combining an extended state observer (ESO) to compensate for the implicit part and a full feed-forward item to eliminate the described part, a hybrid bias-free FCS-MPC is presented. A simple proportional-resonance controller is added to the bias-free FCS-MPC to ease the outer loop design. Contributions of this work include:

1) We mathematically reveal the cause of the tracking bias and split it into (a) *current distortion*, caused by the power grid as the extra input, and (b) *nonlinear impacts* led by discretization of reference state cumulative error, etc. This bridges the discrete FCS-MPC design process and existing tools of system analysis seamlessly (See Section IV).
2) A new bias-free MPC is proposed, which is capable of eliminating biases caused *both* by the grid voltage influences *and* the unmodelled disturbances, simultaneously (See Sub-Sec. B, C of Sec. IV).
3) The proposed bias-free MPC is realized at off-the-shelf hardware and verified at a lab. built setup at different testing scenarios (See Sub-Sec. B, C in Sec. V).

Section II describes the mathematical model of LCL-filtered voltage source converter. Section III presents classically used MPC method, i.e., the predictive current-voltage control, for the underlying system. In Section IV, we mathematically reveal the cause of the tracking biases and propose a new bias-free MPC solution. Section V presents verification data and analysis. Section VI concludes this work.

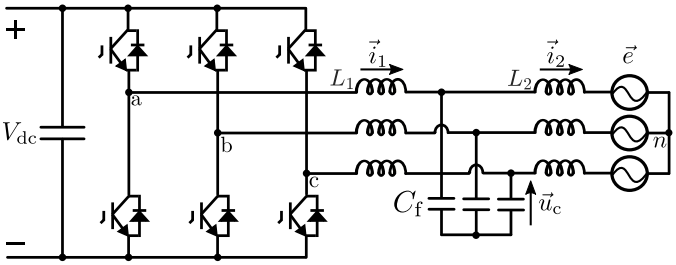

Fig. 2: Two-level grid-tied VSC model with the LCL filter.

II. System Description and Modeling

A two-level voltage source converter (VSC) with LCL-filter is shown in Fig. 2, which is one of the commonly used converters in power electronics. Its control methods can be easily extended to other multi-level power converters, with few modifications. For simplicity, we will choose this topology to show the proposed strategy. According to the diagram of topology in Fig. 2, the system is modeled in the abc, $\alpha\beta$, or dq reference frame with three parts, i.e., the two-level VSC, the LCL filter, and the power grid.

A. Two-Level Voltage Source Converter

As shown in Fig. 2, output voltage of VSC is given as [18]:

$$\vec{u}_{\mathrm{inv}} = \begin{pmatrix} u_{\mathrm{an}} & u_{\mathrm{bn}} & u_{\mathrm{cn}} \end{pmatrix}^{\top} = \frac{V_{\mathrm{dc}}}{3} \begin{bmatrix} 2 & -1 & -1 \\ -1 & 2 & -1 \\ -1 & -1 & 2 \end{bmatrix} \vec{S}_{\mathrm{abc}}, \quad (1)$$

[1]Note that, for the MPC controller design process, its reference input comes from an internal reference generation/calculation process, which is model-based and depends on the parameters of filter (See Sec. IV).

[2]Here the physical relationship between input and output of FCS-MPC is simplified as a precisely description part with another nonlinear disturbance state.

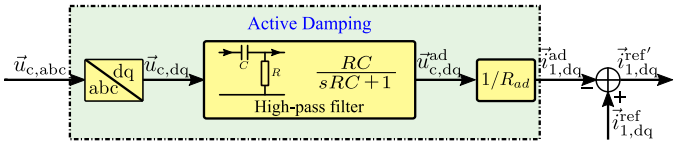

Fig. 3: Control diagram of active damping.

where $\vec{S}_{\rm abc} = (S_{\rm a}, S_{\rm b}, S_{\rm c})^\top$ represents the switching states, and $S_{\rm x} = 1$ (upper switch on, lower switch off) or 0 (upper off, lower on) ($x \in \{\rm a, b, c\}$). $\vec{v}_{\rm inv}$ and $V_{\rm dc}$ are the VSC output and DC-link voltage, respectively. $V_{\rm dc}$ acts on the AC side by different switching states.

B. LCL-filter

The LCL-filter is composed of three parts, i.e. converter and grid side inductors L_1, L_2 with their parasitic resistance R_1 and R_2, and the middle capacitor $C_{\rm f}$, whose resonance frequency and Bode diagram compared with L-filter is shown in Eq. (2) and Fig. 4 (a), respectively.

$$f_{\rm res} = \frac{1}{2\pi}\sqrt{\frac{L_1 + L_2}{L_1 L_2 C_{\rm f}}}. \tag{2}$$

In Fig. 2, $\vec{i}_1$, $\vec{i}_2$, $\vec{u}_{\rm c}$, $\vec{v}_{\rm inv}$, $\vec{e}$ represent the converter and grid side currents, filter capacitor, converter output and the grid voltages, respectively. Based on the *Clark*, *Park* transformation, and the Kirchhoff laws, the LCL-filter mathematical model is shown in dq and $\alpha\beta$ frame.

$$\begin{cases} \dot{\vec{x}}^{\rm dq} = (\mathbf{A} - j\omega\mathbf{I})\vec{x}^{\rm dq} + \mathbf{B}\vec{u}^{\rm dq} \\ \dot{\vec{x}}^{\alpha\beta} = \mathbf{A}\vec{x}^{\alpha\beta} + \mathbf{B}\vec{u}^{\alpha\beta} \end{cases}, \tag{3}$$

where $\begin{cases} \vec{x}^{\rm dq} = (\,\vec{i}_1^{\rm dq}\ \vec{i}_2^{\rm dq}\ \vec{u}_{\rm c}^{\rm dq}\,)^\top \\ \vec{x}^{\alpha\beta} = (\,\vec{i}_1^{\alpha\beta}\ \vec{i}_2^{\alpha\beta}\ \vec{u}_{\rm c}^{\alpha\beta}\,)^\top \end{cases}$ and $\begin{cases} \vec{u}^{\rm dq} = (\,\vec{v}_{\rm n}^{\rm dq}\ \vec{e}^{\rm dq}\,)^\top \\ \vec{u}^{\alpha\beta} = (\,\vec{v}_{\rm n}^{\alpha\beta}\ \vec{e}^{\alpha\beta}\,)^\top \end{cases}$,

matrix $\mathbf{A}$ and $\mathbf{B}$ are:

$$\mathbf{A} = \begin{bmatrix} -\frac{R_1}{L_1} & 0 & -\frac{1}{L_1} \\ 0 & -\frac{R_2}{L_2} & \frac{1}{L_2} \\ \frac{1}{C_{\rm f}} & -\frac{1}{C_{\rm f}} & 0 \end{bmatrix}, \mathbf{B} = \begin{bmatrix} \frac{1}{L_1} & 0 & 0 \\ 0 & -\frac{1}{L_2} & 0 \end{bmatrix}^\top. \tag{4}$$

C. Discretization

FCS-MPC requires a discrete-time system model to predict the future value of state variables. According to Eq. (3) and (4), the output current i_2 is independent of $v_{\rm inv}$ in continuous system. After discretization, the output current is controllable by state variables in the discrete-time domain.

$$\underbrace{\begin{pmatrix} i_{1[{\rm k}+1]} \\ i_{2[{\rm k}+1]} \\ u_{{\rm c}[{\rm k}+1]} \end{pmatrix}}_{\vec{x}_{[{\rm k}+1]}} = \mathbf{\Phi}_{3\times3} \underbrace{\begin{pmatrix} i_{1[{\rm k}]} \\ i_{2[{\rm k}]} \\ u_{{\rm c}[{\rm k}]} \end{pmatrix}}_{\vec{x}_{[{\rm k}]}} + \mathbf{\Gamma}_{3\times2} \underbrace{\begin{pmatrix} u_{{\rm inv}[{\rm k}]} \\ e_{[{\rm k}]} \end{pmatrix}}_{\vec{u}_{[{\rm k}]}}, \tag{5}$$

where $\mathbf{\Phi} = e^{\mathbf{A}T_{\rm s}}$, $\mathbf{\Gamma} = \int_0^{T_{\rm s}} e^{\mathbf{A}\tau}\mathbf{B}d\tau$.

For the grid-tied power converters with LCL-filter, the main objective for the inner loop is to track the given current references, accurately in both steady-state and transient processes. Potential resonance and oscillations shall be damped effectively, within the permissible current and voltage ratings.

Note that, in this work sampling frequency is 25kHz. The fundamental component (50Hz) change is negligible within a sampling period, therefore we assume the following, $\vec{i}^{\rm ref}_{2,{\rm dq}[{\rm k}]} \approx \vec{i}^{\rm ref}_{2,{\rm dq}[{\rm k+1}]}$ and $\vec{u}^{\rm ref}_{{\rm c,dq}[{\rm k}]} \approx \vec{u}^{\rm ref}_{{\rm c,dq}[{\rm k+1}]}$ will hold true.

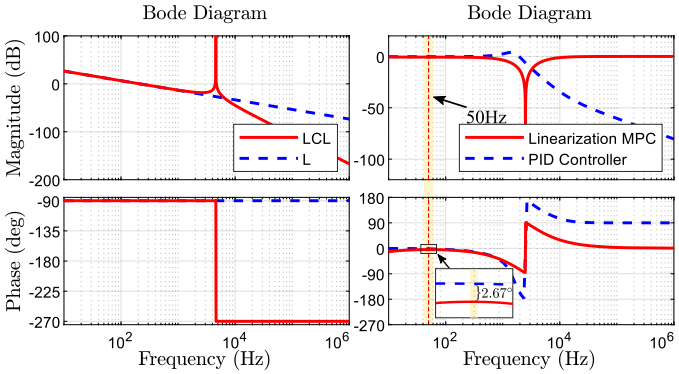

Fig. 4: Bode diagram of (a) LCL- and L-filter, (b) PID control and predictive current-voltage control scheme after modelization.

III. Predictive Current-Voltage Control

With a simple control structure and fast control dynamics, FCS-MPC has received more and more attention. In this part, the classical predictive current-voltage control, targeting to achieve the above control objectives, is firstly revisited, the structure of which is shown in Fig. 6 (c), where $\vec{x}$ represents the converter side current $\vec{i}_1$, capacitor voltage $\vec{u}_{\rm c}$, or the grid side current $\vec{i}_2$.

A. Predictive Current-Voltage Control

Predictive current-voltage control contains three parts, i.e., reference generation, active damping, and cost function [19].

1) Reference Generation: Generally, predictive current-voltage control regulates the output current $\vec{i}_2$ through the converter side current $\vec{i}_1$, the filter capacitor voltage $\vec{u}_{\rm c}$, and the grid side current $\vec{i}_2$[3]. Thus, building the relationship between the $\vec{i}_1^{\rm ref}$ (directly controlled) and given $\vec{i}_2^{\rm ref}$ (actual output) reference is required. According to Eq. (3), relationship among $\vec{i}_2^{\rm ref}$, $\vec{i}_1^{\rm ref}$ and the (inner) variable references can be put as:

$$\begin{cases} \vec{u}^{\rm ref}_{{\rm c,dq[k]}} = \vec{e}_{\rm dq[k]} + R_2 i^{\rm ref}_{2,{\rm dq[k]}} + j\omega L_2 \vec{i}^{\rm ref}_{2,{\rm dq[k]}} \\ \vec{i}^{\rm ref}_{1,{\rm dq[k]}} = \vec{i}^{\rm ref}_{2,{\rm dq[k]}} + j\omega C_{\rm f} \vec{u}^{\rm ref}_{{\rm c,dq[k]}} \end{cases}, \tag{6}$$

where $\vec{i}_2^{\rm ref}$ is the a given reference, the grid voltage $\vec{e}_{\rm dq[k]}$ is known through measurements, and its change is negligible within a very small sampling period $T_{\rm s}$, i.e., $\vec{i}_{2,{\rm dq[k]}} \approx \vec{i}_{2,{\rm dq[k+1]}}$ and $\vec{u}_{{\rm c,dq[k]}} \approx \vec{u}_{{\rm c,dq[k+1]}}$.

2) Cost Function: Considering the calculation time, a delay compensation is used. The system cost function to cope with the aforementioned control objectives, is designed as:

$$\begin{aligned} J_2 =& (i^{\rm ref}_{1,\alpha} - i^{\rm p}_{1,\alpha[{\rm k+2}]})^2 + (i^{\rm ref}_{1,\beta} - i^{\rm p}_{1,\beta[{\rm k+2}]})^2 \\ &+ \lambda_{\rm g}\left[(i^{\rm ref}_{2,\alpha} - i^{\rm p}_{2,\alpha[{\rm k+2}]})^2 + (i^{\rm ref}_{2,\beta} - i^{\rm p}_{2,\beta[{\rm k+2}]})^2\right] \\ &+ \lambda_{\rm c}\left[(u^{\rm ref}_{{\rm c},\alpha} - u^{\rm p}_{{\rm c},\alpha[{\rm k+2}]})^2 + (u^{\rm ref}_{{\rm c},\beta} - u^{\rm p}_{{\rm c},\beta[{\rm k+2}]})^2\right] \end{aligned}, \tag{7}$$

where $\lambda_{\rm g}$, $\lambda_{\rm c}$ are the weighting factors [11], [20]. The reference (converter/grid side current $i_1^{\rm ref}$/$i_2^{\rm ref}$, capacitor voltage $u_{\rm c,}^{\rm ref}$) generation is shown in (6), with corresponding i_1,i_2 and $u_{\rm c,}$ obtained from measurements.

[3]Note that, output current $\vec{i}_2$ cannot be directly manipulated by the switching states [20].

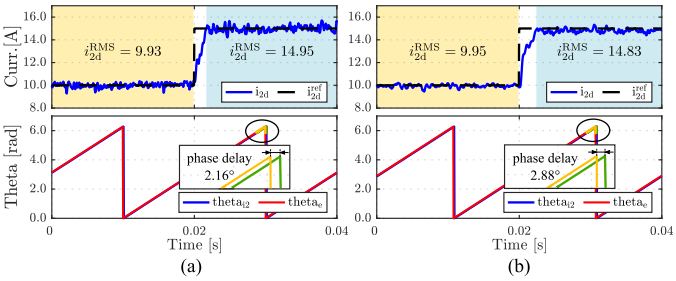

Fig. 5: Active grid side current and its electrical phase in (a) simulation and (b) experiment.

3) Active Damping: For the underlying system, a proper active damping (AD) method is required when some variables are out of control (λ_g and/or λ_c=0) [20]. It simulates a damping resistance R_{ad} in parallel with capacitor voltage u_c, realized by adding an extra term in converter side current reference, as Eq. (8) indicates.

$$i_1^{ref'} = i_1^{ref} - \frac{1}{R_{ad}} u_c, \tag{8}$$

where R_{ad} is the virtual damping resistance, $i_1^{ref'}$ is the output reference. Fig. 3 shows control diagram of AD with the capacitance voltage feedback. Subtracting the damping item $i_{1,dq}^{ad}$, the converter side current reference is derived as $i_{1,dq}^{ref'}$.

B. Discussion

As shown in Eq. (6), widely applied predictive current-voltage control needs a progressive discrete reference generation based on filter model. In this process, $\vec{u}_{c,dq[k]}^{ref}$ contains the discrete grid current reference $\vec{i}_{2,dq}^{ref}$ error ($\vec{i}_{2,dq[k]}^{ref} \approx \vec{i}_{2,dq[k+1]}^{ref}$), while the $\vec{i}_{1,dq[k]}^{ref}$ includes the error existed in the capacitor voltage reference $\vec{u}_{c,dq[k]}^{ref}$ ($\vec{u}_{c,dq[k]} \approx \vec{u}_{c,dq[k+1]}$), which is accumulated based on given $\vec{i}_{2,dq[k]}^{ref}$. Thus, nonlinear nature of FCS-MPC impedes the analysis of underlying system under linear tools.

Fig. 5 shows the simulated and experimental result comparison of grid side current in abc-axis and its electrical phase. Considering the predictive current-voltage control, it clearly shows the tracking bias (active grid current error: 0.05A, 0.17A under 15A reference; phase error: 2.16°, 2.88°, respectively) exists in both simulated and experimental grid side current (Testing scenarios and parameters are shown in Sec. V).

IV. The Proposed Bias-Free Predictive Control

From the discussion above, classical predictive current-voltage control fails to control the underlying system in mitigating tracking bias and at the imprecise MPC modelization. In the following, we firstly reveal the cause of existed internal tracking bias, mathematically. Thereafter, we introduce a new bias-free FCS-MPC technique and its key realization steps.

A. Mathematical Formulation of the Tracking Biases

Follow analysis split tracking bias into *linear item* (grid disturbances) and *nonlinear implicit impact* to model or observe.

1) **Grid Disturbances:** Generally, nonlinear loads and power grid connect to the grid-tied converter through point of common coupling, while the grid, as an extra input of underlying system, distorts the output current. This distortion has been totally studied and modeled [10].

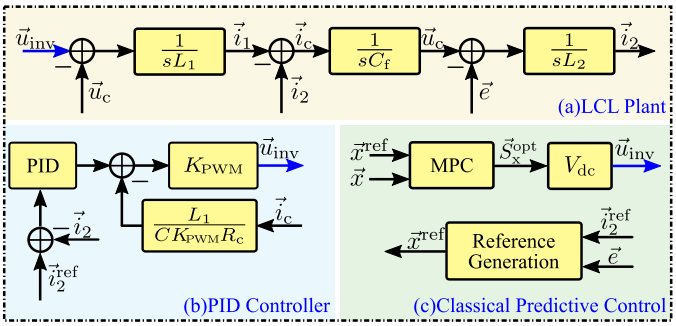

Fig. 6: PID control and predictive current-voltage control scheme for 2L-VSC with LCL filter.

As for FCS-MPC, the unavoidable distortion is hard to get the transfer function between the output ($\vec{i}_2$) and inputs ($\vec{i}_2^{ref}$ and $\vec{e}$) for the underlying system, as shown in Fig. 6 (a) and (c). The key reason is that MPC cannot be analyzed under a unified framework with other linear blocks. Aiming at this problem and based on the physical relationships between inputs and output of FCS-MPC, we approximately model the linear part of the predictive control block, as shown in Fig. 7, while the active damping link is added in the equivalent model because the predictive current-voltage control can inherently dampen the resonance. According to the *superposition principle*[4], FCS-MPC can be unified with other linear part, like reference generation process and LCL-filter, under linear analysis.

Thus, the grid disturbance can be summarized in Eq. (9) (linear part). The nonlinear impacts existed in FCS-MPC will be discussed in the following subsection. The Bode diagram for comparison of Eq.(9) reference tracking and grid disturbance part with PID controller (Fig. 6 (b)) is shown in Fig. 4 (b), which clearly indicates the FCS-MPC has a more severe static bias than classical linear controller.

2) **Equivocation of Implicit Impacts:** Except the disturbance caused by grid voltage, the inner state reference cumulative error also acts on output current bias, while the approximate MPC modelization leads to imprecise analysis. As the discussion in **Sec. III (B)**, nonlinear tracking nature of FCS-MPC lends the discrete cumulative error hard to model in an mathematical representation like the grid disturbance. Therefore, we define the reference cumulative error and the other implicit impacts as a outer unknown input $d(s)$ totally, injecting into the FCS-MPC output u_{inv}. Thus, except the nonlinear injection, the underlying system can be put into an unified framework with the other linear part to be analyzed by *superposition principle*. The transfer function between the output current and inputs is shown as:

$$i_2(s) = \overbrace{e^{-1.5sT_s}\left(1 + \frac{G_{x1}(s)}{T_A(s)}\right) i_2^{ref}(s)}^{\text{reference tracking}} + \overbrace{\frac{G_{x2}(s)}{T_A(s)} e(s)}^{\text{grid disturbance}} + \overbrace{\frac{R_c}{T_B} d(s)}^{\text{nonlinear impacts}}, \tag{9}$$

where T_s is the sampling time. $e^{-1.5sT_s}$ is the sampling and transport delay, while $d(s)$ is the sets of nonlinear reference cumulative error and other implicit impacts in the frequency-domain. $T_A(s)$, $T_B(s)$, $G_{x1}(s)$, $G_{x2}(s)$ is shown in Eq. (14).

[4]For all linear systems, the response caused by multi-stimuli is the sum of the responses caused by each stimulus individually.

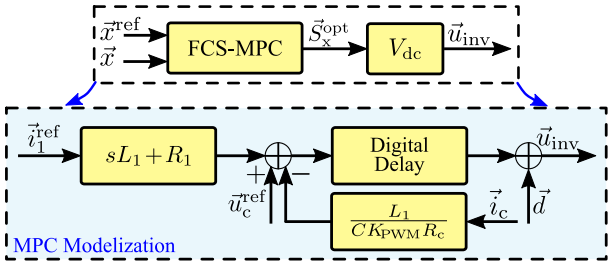

Fig. 7: FCS-MPC approximation modelization scheme.

B. Proposed Hybrid Bias-Free FCS-MPC

In the following, we implement the bias-free methods under $\alpha\beta$ reference frame. Eq. (9) shows that the tracking bias has two parts, i.e. nonlinear inner state reference cumulative error, and linear grid disturbance. In this paper, we propose an observer based on ESO to compensate for the nonlinear impacts $\frac{R_c}{T_B}d(s)$. The error caused by the grid influence $\frac{G_{x2}(s)}{T_A(s)}e(s)$ is compensated with a full feed-forward method. Fig. 9 (a) shows this hybrid bias-free FCS-MPC diagram.

1) **Observer Design:** In Eq. (9), the nonlinear state reference tracking bias item, $\frac{R_c}{T_B}d(s)$, cannot be expressed mathematically. It collects the nonlinear accumulated reference error and other implicit impacts, like model uncertainty. ESO is an effective solution to observe the system state and external disturbance totally without dependence on the mathematical model. Assuming that $e^{-1.5sT_s}$ is equal to 1 under 50Hz, Fig. 7 shows the relationship between $\vec{u}_{inv}^{ref}$ and the $\vec{u}_{inv}$:

$$\begin{cases} \frac{d\vec{i}_1^{ref}}{dt} = \frac{1}{L_1}\vec{u}_{inv} + F \\ F = \frac{1}{L_1}(\vec{d} - \vec{u}_c^{ref}) \end{cases}, \tag{10}$$

where the F is considered as the total disturbance, including the nonlinear accumulated reference error and other implicit impacts. Based on this, a linear ESO is constructed as follows:

$$\begin{cases} e_{rr} = \hat{i}_1^{ref} - i_1^{ref} \\ \dot{\hat{i}}_1^{ref} = \alpha\vec{u}_{inv} + \hat{F} - \beta_1 e_{rr} \\ \dot{\hat{F}} = -\beta_2 e_{rr} \end{cases}, \tag{11}$$

where the e_{rr}, $\alpha = \frac{1}{L_1}$, $\hat{i}_1^{ref}$, $\hat{F}$ are the observer error, the gain of the input value, estimation of i_1^{ref} and F; β_1, β_2 are the feedback gain of the observer. In the digital controller, the ESO is discretized as Eq. (11) shown:

$$\begin{cases} e_{rr[k]} = \hat{i}_{1[k]}^{ref} - i_{1[k]}^{ref} \\ \hat{i}_{1[k+1]}^{ref} = \hat{i}_{1[k]}^{ref} + T_s(\alpha\vec{u}_{inv[k]} + \hat{F}_{[k]} - \beta_1 e_{rr[k]}) \\ \hat{F}_{[k+1]} = \hat{F}[k] - T_s\beta_2 e_{rr[k]} \end{cases}. \tag{12}$$

According to, β_1 and β_2 affect the stability of ESO and need to be designed . We obtain the transfer function for the continuous Eq. (11) and discrete Eq. (12) ESO as follows:

$$\begin{cases} G(s) = \frac{\hat{i}_1^{ref}}{i_1^{ref}} = \frac{\beta_1 s + \beta_2}{s^2 + \beta_1 s + \beta_2} \\ G(z) = \frac{\hat{i}_1^{ref}(z)}{i_1^{ref}(z)} = \frac{\beta_1 T_s(z-1) + \beta_2 T_s^2}{(z-1)^2 + \beta_1 T_s(z-1) + \beta_2 T_s^2} \end{cases}. \tag{13}$$

The characteristic equation can be expressed as:

$$\begin{cases} T_A(s) = s^3 C_f L_1 L_2 R_c + s^2 L_1 L_2 + sR_c(L_1 + L_2) \\ T_B(s) = s^3(C_f L_1 L_2 R_c + L_1^2 L_2) + s^2 L_1 L_2(1 + R_1) + sR_c(L_1 + L_2) \\ G_{x1}(s) = s^2[C_f R_c(L_1 R_2 + L_2 R_1)] + sC_f R_c R_1 R_2 + R_c(R_1 + R_2) \\ G_{x2}(s) = e^{-1.5sT_s}(s^2 C_f L_1 L_2 + sC_f L_1 R_2 + e^{-1.5sT_s} C_f R_c R_2) \end{cases}. \tag{14}$$

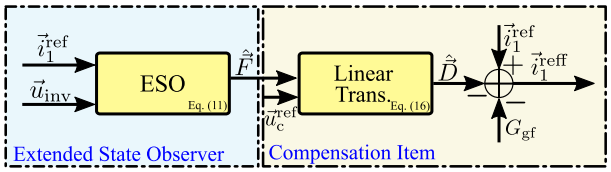

Fig. 8: Hybrid bias-free method.

$$\begin{cases} C(s) = s^2 + \beta_1 s + \beta_2 \\ C(z) = (z-1)^2 + \beta_1 T_s(z-1) + \beta_2 T_s^2 \end{cases}. \tag{15}$$

For the $C(s)$, both roots is able to fall at $-\omega_0$, which means $\beta_1 = 2\omega_0$ and $\beta_w = \omega_0^2$, where $-\omega_0$ is the bandwidth of ESO. Thus, the design process of β_1 and β_2 can be simplified as the design of ω_0, while the $C(z) = 0$ solves the poles in z domain: $z = 1 - \omega_0 T_s$. The ω_0 is calculated as $\omega_0 = \frac{(1-z)}{T_s}$.

In general, the practical optimality of the observer is to increase the bandwidth within the limitation of noises and fixed sampling rate. Larger ω_0 will introduce more noise into ESO, even leading to system divergence. And smaller ω_0 also leads to bad dynamic performance. In this paper, we set $z = 0.7$ and $\omega_0 = 17500$ with 25kHz sampling frequency.

Besides, as shown in Fig. 7, directly acting on the u_{inv}, the compensation item $\vec{d}_{[k+1]}$ can not be added into the i_1^{ref}. Hence, through a series of equivalent block transform, $\vec{d}_{[k+1]}$ is transformed into $D_{[k+1]}$ from the output of u_{inv}^{ref} to the i_1^{ref}, as shown in Fig. 8. The transformation function is shown as:

$$\begin{cases} d_{[k]} = L_1\dot{\hat{F}}_{[k]} + u_c^{ref} \\ D_{[k+1]} = T_s d_{[k]} + (1 - T_s\frac{R_1}{L_1})D_{[k]} \end{cases}, \tag{16}$$

where the $D_{[k+1]}$ is the compensation item added in i_1^{ref}.

2) **Full Feed-Forward Item:** Except the nonlinear accumulated reference error, grid disturbance also needs to be eliminated. Mathematical expression of grid disturbance has been shown in Eq. (9). Researchers have proposed an effective solution, *full feed-forward method*, to eliminate grid influence reflected in output current of LCL-filtered converters [10]. It counteract the disturbance through equivalent block transform in frequency-domain. In the proposed system, we already knows the grid disturbance expression $\frac{G_{x2}(s)}{T_A(s)}e(s)$ in Eq. (9). The additional feed-forward path, as shown in Fig. 9 (a),is introduced where the node of e is moved from u_c to i_1^{ref} with gain of $G_{gf}(s)$, which is expressed as follows:

$$\begin{aligned} G_{gf}(s) =& s(\frac{C_f}{e^{-1.5sT_s}} - C_f + \frac{L_2}{R_c}) + \\ & \frac{1}{sL_1}(\frac{1}{e^{-1.5sT_s}} - 1) + \frac{1}{e^{-1.5sT_s}R_c}. \end{aligned} \tag{17}$$

Besides, the $e^{-1.5sT_s}$ can be simplified as 1 under 50 Hz. So the transfer function is as follows:

$$G_{gf}(s) = s\frac{L_2}{R_c} + \frac{1}{R_c}. \tag{18}$$

Therefore, except nonlinear error compensation term $D_{[k+1]}$ (Eq. (16)), we add grid disturbance offset item $(G_{gf} \cdot e)_{[k+1]}$ (Eq. (17)) in the i_1^{ref}, as Fig. 8 shows. Section V demonstrates the simulated and experimental performance of the hybrid bias-compensation FCS-MPC diagram.

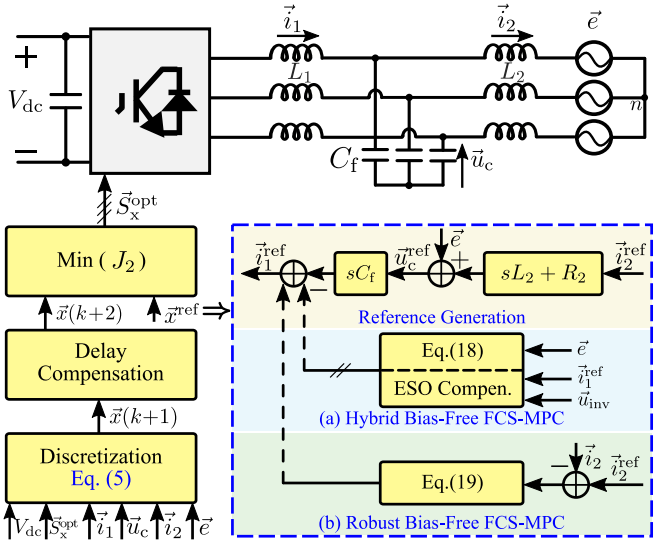

Fig. 9: Proposed bias-free FCS-MPC method.

3) **Key Realization Steps:** For the control of mentioned LCL-filtered converters, FCS-MPC is an effective alternative, but the tracking bias exists in the output current. Focusing on the problem, we propose a bias-free FCS-MPC method, whose key realization steps is shown in Algorithm 1.

C. Simplified Outer Loop Design

1) Outer Loop Design: Based on ESO and full-feed-forward method, the proposed hybrid bias-free FCS-MPC has complicated control structure. To overcome the problem, we simplify the outer compensation loop design, named as robust bias-free FCS-MPC. Fig. 9 shows the diagram of the robust bias-free FCS-MPC. The output current error regulation item, a PR controller, is added into the i_1^{ref} reference, which replaces the ESO and full feed-forward term, whose formulation $G_{\mathrm{ff}}^{'}(s)$ is expressed as follows:

$$G_{\mathrm{ff}}^{'}(s) = K_{\mathrm{p}} + \frac{2K_{\mathrm{r}}\omega_{\mathrm{c}}s}{s^2 + 2\omega_{\mathrm{c}}s + \omega_{\mathrm{o}}^2}, \tag{19}$$

where the K_{p}, K_{r} are the proportional gain, resonant gain, resonant cut-off frequency, respectively. ω_{c} represents the width of side-band around resonant frequency and limits the quality factor of the resonant term, while ω_{o} is the center of the resonant term which is equal to 100π. Now, Eq. 19 summarizes the whole proposed structure.

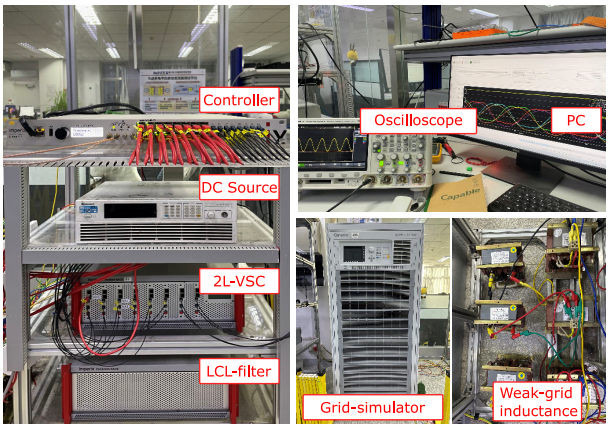

Fig. 10: Test bench setup for verifying the proposed methods.

Algorithm 1 Framework of hybrid bias-free FCS-MPC.

Step I: Observe $\hat{F}_{[\mathrm{k}+1]}$ and transform into $D_{[\mathrm{k}+1]}$, Eq. (16).
Step II: Sample $e_{[k]}$ and compute $(G_{\mathrm{gf}} \cdot e)_{[k]}$, Eq. (18).
Step III: Add $D_{[k+1]}$ and $(G_{\mathrm{gf}} \cdot e)_{[k]}$ into the i_2^{ref}, Fig. 8.
Step IV: Apply the reference(s) to predictive optimal gate signal vector $\vec{u}_{\mathrm{inv}[k+1]}$, Fig. 9 (b).

2) Discussion: The proposed hybrid bias-free FCS-MPC can precisely express and compensate for the output current bias in the last subsection. However, it definitely needs a bias-free solution, i.e., ESO and full feed-forward method, while the model-based error compensation solution is sensitive to variation of parameters or working conditions or equipment. On the other hand, closed-loop-based compensation can effectively improve the robustness of the FCS-MPC method when the system has parameter variation. Thus, a simple proportional-resonance controller is added to ease the outer loop design, forming a *robust bias-free FCS-MPC* without bias. The static and dynamic performance of robust bias-free FCS-MPC is verified in Section V.

V. Effectiveness Verification

In this section, classical PID control with AD, predictive current-voltage control, proposed bias-free FCS-MPC strategy for grid-tied LCL-filtered converter are validated by simulation and experiment data. The parameters of the setup are collected in Table I, where the simplified outer loop gain and weighting factors are tuned with the solutions proposed in [21] and [11], [20], respectively. Simulation is done via the PLECS environment, while the controller hardware for the experimental verification is B-BOX-RCP, an off-the-shelf product from Imperix. The power part of the test-bench is composed of silicon carbide Metal-Oxide-Semiconductor Field-Effect Transistor (MOSFET) phase-leg power module, passive filters, a DC source, and an AC grid. Fig. 10 shows the experimental hardware platform for the controller and VSC connected to the grid through LCL-filter.

A. Overall Evaluation

To verify the overall control performance of the proposed solution, we set testing scenarios as follows. The active current reference $i_{\mathrm{d}}^{\mathrm{ref}}$ is changed from 10A to 15A , 10A at 0.25s, 0.75s, while the reactive current reference $i_{\mathrm{q}}^{\mathrm{ref}}$ is changed from

TABLE I: System Parameters.

Parameters	Symbols	Values
Fundamental frequency	f_{nom}	50 Hz
Sampling time	T_{s}	40 μs
Grid voltage	e (RMS)	30 V
DC voltage	V_{dc}	100 V
Converter-side inductor	L_1	2.5 mH
Converter-side parasitic resistance	R_1	22 mΩ
Grid-side inductor	L_2	2.5 mH
Grid-side parasitic resistance	R_2	22 mΩ
Filter capacitor	C_{f}	3 μF
Weighting factor of i_2	λ_{g}	2.5
Weighting factor of u_{c}	λ_{c}	0.015
Proportional gain	K_{p}	0.1
Resonant gain	K_{r}	10
Resonant cut-off frequency	ω_{r}	5

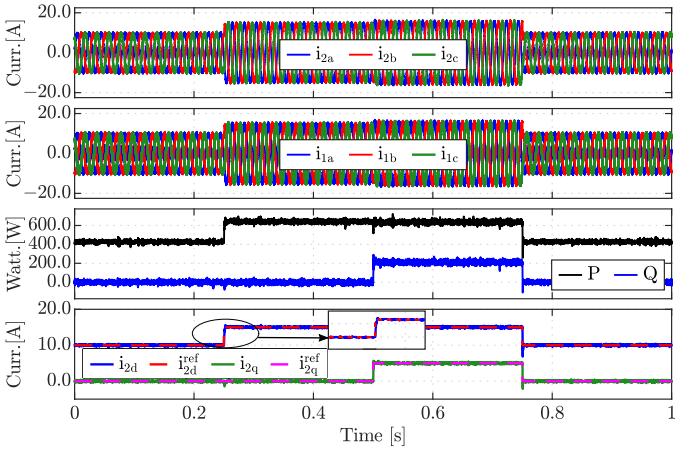

Fig. 11: Overall experimental performances of the proposed robust bias-free FCS-MPC. From up to the down: (a) grid-side current i_2, (b) converter-side current i_1, (c) output active and reactive power, (d) i_2 on dq-axis.

0A to 5A and 0A at 0.5s, 0.75s, respectively. The results are collected in Fig. 11, where it can be seen that the proposed solution achieves global stability, good steady and dynamic performances. Particularly, the current tracking at different large-scale reference changes is precise and stable.

B. Comparison of the Classical and Proposed Solutions

Test scenarios are set as follows to compare the transient and steady state control performances of the (i) PID control with active damping (AD), (ii) predictive current-voltage control, and (iii) hybrid bias-free (iv) robust bias-free FCS-MPC.

1) Steady State Performances: Steady state performances of four methods, in terms of the grid current quality (indicated via total-harmonic distortions, THDs) and tracking bias (indicated via phase delay) are shown in Fig. 13 (a), (b). As can be clearly seen, grid side current has low THD (2.095%, 2.221%, 2.011%, 2.219% for (i-iv)). Predictive current-voltage control has a 2.16° phase bias. The other solutions did not show tracking bias. Note that, as shown in Fig. 12, the PID controller has comparable static performance (approximate THD) but a higher switching frequency (5kHz>3.7kHz) than the predictive control, further confirming the effectiveness of the proposal in eliminating tracking biases.

2) Dynamic State Performances: The dynamic output performances (indicated via transient time) of these four methods are shown in Fig. 13 (b). It displays that FCS-MPC-based shows fast transient performances (0.01600s, 0.00504s, 0.00464s,0.00456s for (i-iv)), which reveals the bias-free solutions will not worsen the dynamic performance.

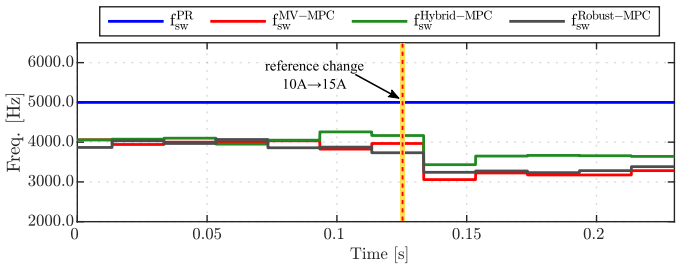

Fig. 12: Switching frequency of PID control, predictive current-voltage control, hybrid bias-free FCS-MPC, and robust bias-free FCS-MPC (f_{sw}=5kHz, ≈3637Hz, 3695Hz, 3659Hz, respectively). Operating condition is same as Fig. 13 (b).

TABLE II: Performance Comparison at Parameter Deviations

	Method	THD (%)	Phase Delay (°)
$L_2^{\text{controller}}$ =0.5L_2^{real}	Classical MPC[1]	1.673	2.16
	Proposed MPC 1[2]	1.601	-1.44
	Proposed MPC 2[3]	1.584	0
$L_2^{\text{controller}}$ =2L_2^{real}	Classical MPC[1]	2.321	2.16
	Proposed MPC 1[2]	2.325	1.44
	Proposed MPC 2[3]	2.283	0

[1] Predictive Current-Voltage Control.
[2] Hybrid bias-free FCS-MPC.
[3] Robust bias-free FCS-MPC.

Notably, FCS-MPC methods have similar switching frequencies f_{sw} with the same control intervals. The data of f_{sw} is shown via Fig. 12. The comparison with PID controller verifies the credibility of predictive control in reducing switching losses, where f_{sw} is less than 1/5 of sampling frequency.

3) Performance Comparison at Parameter Deviations: For the model-based methods, parameter deviations, especially the grid-side inductance mismatches, are unavoidable. The testing scenarios for this condition is that, $L_2^{\text{controller}}$ is set as 50% or 200%L_2^{real} in the controller, to create a large enough mismatch. We collect the experimental data of all the aforementioned solutions in Table II, showing both the tracking biases and current quality (THDs) comparison. It confirms that, the proposed solution outperforms predictive current-voltage control considerably, while only robust bias-free MPC compensates for the tracking bias against the parameter mismatches.

To sum up, in order to illustrate the superiority of the proposed methods, we compare the static and dynamic results of four methods in Fig. 13. It sufficiently proves that the proposed bias-free methods eliminate the tracking bias efficiently. Meanwhile, the proposed methods are robust enough against parameter deviations without other performance sacrificed.

C. Abnormal Grid Tests

Weak-grid-connected and grid-harmonic-injection conditions are necessarily considered converter control situations, e.g., renewable energy grid-tied problem, micro AC grids, etc.

1) Weak-Grid-Connected Condition: Weak-grid-connected condition is one of the most common abnormal grid situations, which could be generally simplified as the grid in series with an inductance L_{g}[5]. Fig. 14 shows experimental waveforms under L_{g} =5mH (200%L_2) when applying robust bias-free FCS-MPC. Under worse PCC voltage, proposed method shows robustness against the grid impedance variations with acceptable static or dynamic performance.

2) Grid-Harmonic-Injection Condition: In this condition, 11th-order harmonic (10%e) is injected into the grid-voltage e. As Section IV A analyzed, the changing e will directly affect the output steady and dynamic performance. Fig. 15 shows the experimental waveforms, which indicates that the proposed robust bias-free FCS-MPC tolerates well with grid harmonic and is robust enough to adapt to different grid conditions, which is an essential precondition for industrial applications.

[5]Note that, harmonics of PCC voltage under weak-grid-connected condition can be greatly larger than the stiff one.

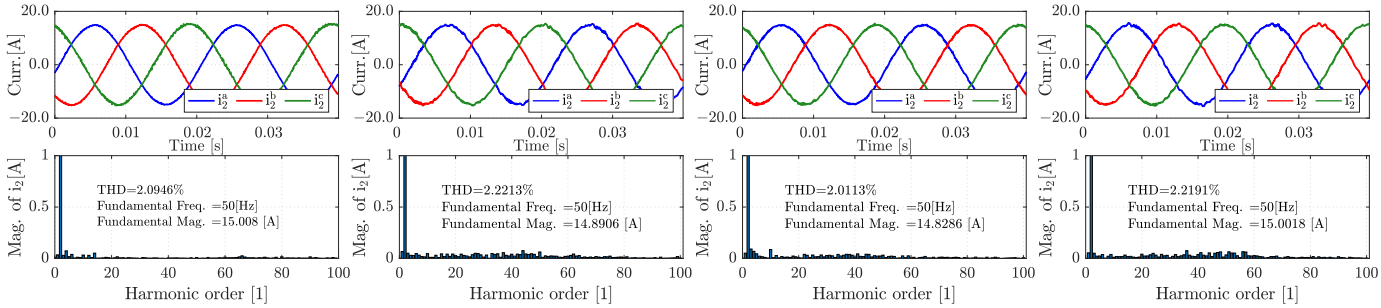

(a) Grid current static performance of PID control with AD, predictive current-voltage control, hybrid bias-free FCS-MPC, and robust bias-free FCS-MPC.

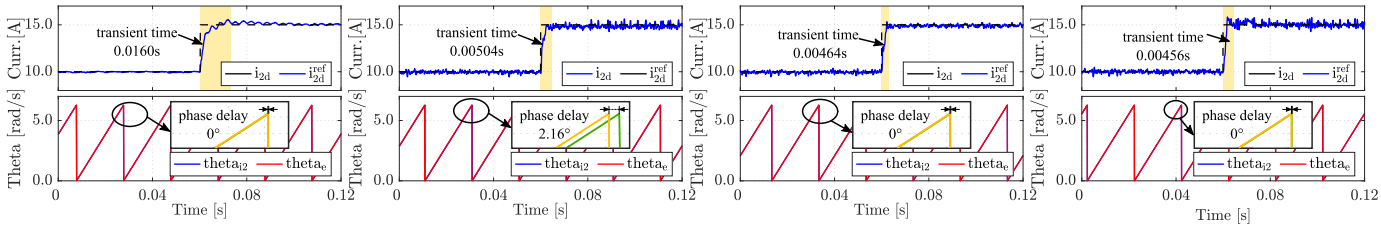

(b) Grid current dynamic and static performance of PID control with AD, predictive current-voltage control, hybrid bias-free FCS-MPC, and robust bias-free MPC.

Fig. 13: Experimental result. Four controller performance comparison. All the experimental results are implemented with same weighting factors.

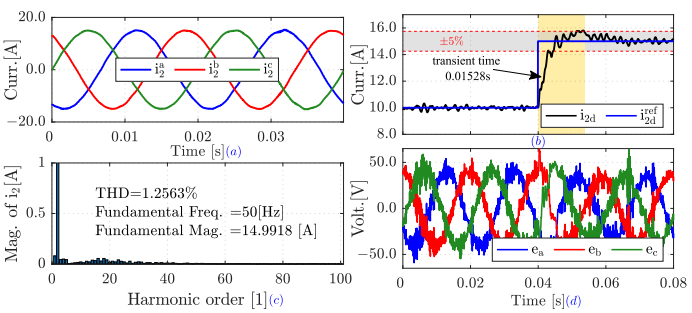

Fig. 14: Experimental result. Grid side current performance (a), (b), (c) and grid voltage performance (d) under weak-grid-connected condition (5mH grid inductance).

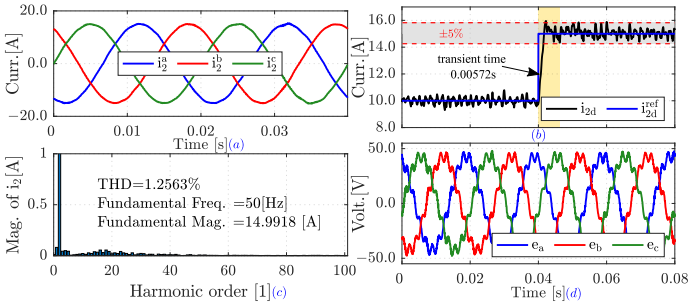

Fig. 15: Experimental result. Grid side current performance (a), (b), (c) and grid voltage performance (d) under 11th-order grid-harmonic-injected (10% rated grid voltage).

VI. Conclusion

Finite-control-set model predictive control (FCS-MPC) is an interesting alternative to control multiple input and multiple output dynamic systems with constraints, e.g., the underlying grid-tied converters with LCL-filter. However, due to grid disturbances and the nonlinear reference cumulative error, steady-state tracking bias exists in the output current when classical predictive current-voltage control is applied. This work provides a direct mathematical solution to express the FCS-MPC, and proposes a new bias-free predictive control for the LCL-filtered grid-tied converters in micro-energy systems. Compared with existing solutions, the proposed method is flexible and robust to different system parameter variations, grid side disturbances, *while* remains fast control dynamics and a simple structure as the classical predictive control, without requiring a modulator.

Future work will focus on the study and extension of the proposed solution to its applications of the interaction of a group of LCL-filtered converters in micro-energy systems.

Acknowledgment

The authors would like to express sincere gratitude to Zhen Li, Xiaozhe Liu, Yu Li from Shandong University, Yongfeng Zhang from University of Jinan, and Yi Zhang from Fuzhou University for their insightful feedback and valuable discussions during the preparation of this paper.

References

[1] M. Al-Gabalawy, A. R. Adly, A. Y. Abdelaziz, and N. S. Hosny, "Micro-energy Systems (MESs); Modeling and Optimal Operating Based on NSGA-II." Springer, 2022, vol. 224, pp. 99–128.

[2] M. Liserre, F. Blaabjerg, and S. Hansen, "Design and control of an LCL-filter-based three-phase active rectifier," *IEEE Transactions on Industry Applications*, vol. 41, no. 5, pp. 1281–1291, 2005.

[3] X. Wang, F. Blaabjerg, and P. C. Loh, "Passivity-Based Stability Analysis and Damping Injection for Multiparalleled VSCs with LCL Filters," *IEEE Transactions on Power Electronics*, vol. 32, no. 11, pp. 8922–8935, 2017.

[4] J. Xu, S. Xie, and T. Tang, "Active damping-based control for grid-connected LCL -filtered inverter with injected grid current feedback only," *IEEE Transactions on Industrial Electronics*, vol. 61, no. 9, pp. 4746–4758, 2014.

[5] J. Dannehl, M. Liserre, and F. W. Fuchs, "Filter-based active damping of voltage source converters with LCL filter," *IEEE Transactions on Industrial Electronics*, vol. 58, no. 8, pp. 3623–3633, 2011.

[6] H. Abu-Rub, J. Guzinski, Z. Krzeminski, and H. Toliyat, "Predictive current control of voltage-source inverters," *IEEE Transactions on Industrial Electronics*, vol. 51, no. 3, pp. 585–593, 2004.

[7] Z. Zhang, C. M. Hackl, and R. Kennel, "Computationally Efficient DMPC for Three-Level NPC Back-to-Back Converters in Wind Turbine Systems with PMSG," *IEEE Transactions on Power Electronics*, vol. 32, no. 10, pp. 8018–8034, 2017.

[8] S. Y. Park, C. L. Chen, J. S. Lai, and S. R. Moon, "Admittance compensation in current loop control for a grid-tie LCL fuel cell inverter," *IEEE Transactions on Power Electronics*, vol. 23, no. 4, pp. 1716–1723, 2008.

[9] T. Abeyasekera, C. M. Johnson, D. J. Atkinson, and M. Armstrong, "Suppression of line voltage related distortion in current controlled grid connected inverters," *IEEE Transactions on Power Electronics*, vol. 20, no. 6, pp. 1393–1401, 2005.

[10] H. Zhang, X. Ruan, Z. Lin, L. Wu, Y. Ding, and Y. Guo, " Capacitor Voltage Full Feedback Scheme for LCL -Type Grid-Connected Inverter to Suppress Current Distortion Due to Grid Voltage Harmonics ," *IEEE Transactions on Power Electronics*, vol. 36, no. 3, pp. 2996–3006, 2020.

[11] C. Xue, D. Zhou, and Y. Li, "Hybrid Model Predictive Current and Voltage Control for LCL-Filtered Grid-Connected Inverter," *IEEE Journal of Emerging and Selected Topics in Power Electronics*, vol. 9, no. 5, pp. 5747–5760, 2021.

[12] T. Dragičević, C. Zheng, J. Rodriguez, and F. Blaabjerg, "Robust Quasi-Predictive Control of LCL-Filtered Grid Converters," *IEEE Transactions on Power Electronics*, vol. 35, no. 2, pp. 1934–1946, 2020.

[13] P. Falkowski and A. Sikorski, "Finite Control Set Model Predictive Control for Grid-Connected AC-DC Converters With LCL Filter," *IEEE Transactions on Industrial Electronics*, vol. 65, no. 4, pp. 2844–2852, apr 2018.

[14] L. Liu, C. Xie, W. Wang, D. Zhou, and J. Zou, "A double-loop robust model predictive control for lcl-type grid-connected inverters," *2021 IEEE International Conference on Predictive Control of Electrical Drives and Power Electronics (PRECEDE)*, pp. 863–868, 2021.

[15] B. Karanayil and M. F. Rahman, "Artificial neural network applications in power electronics and electrical drives," *Power Electronics Handbook*, vol. 54, no. 1, pp. 1015–1030, 2007.

[16] S. Zhao, F. Blaabjerg, and H. Wang, "An Overview of Artificial Intelligence Applications for Power Electronics," *IEEE Transactions on Power Electronics*, vol. 36, no. 4, pp. 1–1, 2020.

[17] D. Wang, Z. J. Shen, X. Yin, S. Tang, X. Liu, C. Zhang, J. Wang, J. Rodriguez, and M. Norambuena, "Model Predictive Control Using Artificial Neural Network for Power Converters," *IEEE Transactions on Industrial Electronics*, vol. 69, no. 4, pp. 3689–3699, 2022.

[18] Z. Zhang, H. Xu, M. Xue, Z. Chen, T. Sun, R. Kennel, and C. M. Hackl, "Predictive Control With Novel Virtual-Flux Estimation for Back-to-Back Power Converters," *IEEE Transactions on Industrial Electronics*, vol. 62, no. 5, pp. 2823–2834, 2015.

[19] J. Rodriguez, P. Cortes, R. Kennel, and M. P. Kazmierkowski, "Model predictive control - A simple and powerful method to control power converters," *2009 IEEE 6th International Power Electronics and Motion Control Conference, IPEMC '09*, vol. 56, no. 6, pp. 41–49, 2009.

[20] N. Panten, N. Hoffmann, and F. W. Fuchs, "Finite Control Set Model Predictive Current Control for Grid-Connected Voltage-Source Converters with LCL Filters: A Study Based on Different State Feedbacks," *IEEE Transactions on Power Electronics*, vol. 31, no. 7, pp. 5189–5200, 2016.

[21] M. A. Ebrahim, B. A. Aziz, M. N. F. Nashed, and F. A. Osman, "Optimal design of proportional-resonant controller and its harmonic compensators for grid-integrated renewable energy sources based three-phase voltage source inverters," *IET Generation, Transmission & Distribution*, vol. 15, no. 8, pp. 1371–1386, 2021.

Qianli Xing (Student Member, IEEE) was born in Shandong, China. He received B.S. degree from the School of Electrical and Power Engineering, Shandong University, China, in 2020. He is currently a Master's degree candidate at the Lab of More Power Electronics Energy Systems, School of Electrical Engineering, Shandong University, China. His research interests include advanced control of LCL-filtered grid-tied power converter in micro-energy systems, etc.

Zhenbin Zhang (Senior Member, IEEE) was born in Shandong, China, in 1984. He received the Ph.D. degree *(summa cum laude)* from the Institute for Electrical Drive Systems and Power Electronics (EAL), Technical University of Munich (TUM), Munich, Germany, in 2016.

From 2016 to 2017, he was a Research Fellow and the Group Leader of the Modern Control Strategies for Electrical Drives Group, EAL, TUM. Since 2017, he has been a Full Professor and the Lab Director with Shandong University, Jinan, China, where he is the Director of the International Center for Intelligent Energy and Power Conversion Systems (IEPCS) since 2020. His research interests include power electronics and electrical drives, sustainable energy systems, smart-grids, and micro-grids. Dr. Zhang received the VDE-Award from Suedbayern, Germany, in 2017. He is also an Associate Editor for the IEEE Transactions on Power Electronics.

Tomislav Dragičević (Senior Member, IEEE) received the M.Sc. and Ph.D. degrees in electrical engineering from the Faculty of Electrical Engineering, University of Zagreb, Zagreb, Croatia, in 2009 and 2013, respectively.

From 2013 until 2016, he has been a Postdoctoral Researcher with Aalborg University, Aalborg, Denmark. From 2016 until 2020, he was an Associate Professor with Aalborg University, Denmark. He is currently a Professor with the Technical University of Denmark, Kongens Lyngby, Denmark. He made a Guest Professor stay with Nottingham University, Nottingham, U.K., during spring/summer of 2018. He has authored and coauthored more than 330 technical publications (more than 150 of them are published in international journals, mostly in IEEE), 10 book chapters and a book in this field, as well as filed for several patents. His research interests include application of advanced control, optimization and artificial intelligence inspired techniques to provide innovative and effective solutions to emerging challenges in design, control, and diagnostics of power electronics intensive electrical distributions systems and microgrids.

Jose Rodriguez (Life Fellow, IEEE) received the engineering degree in electrical engineering from the Universidad Tecnica Federico Santa Maria, Valparaiso, Chile, in 1977, and the Dr.-Ing. degree in electrical engineering from the University of Erlangen, Erlangen, Germany, in 1985.

He has been with the Department of Electronics Engineering, Universidad Tecnica Federico Santa Maria, since 1977, where he was a Full Professor and the President. From 2015 to 2019, he was the President of Universidad Andres Bello, Santiago, Chile. Since 2022, he has been the President of Universidad San Sebastian, Santiago. He has coauthored two books, several book chapters, and more than 700 journal and conference papers. His main research interests include multilevel inverters, control of power converters, and adjustable-speed drives. He is a member of the Chilean Academy of Engineering. He has received a number of best paper awards from journals of the IEEE. In 2014, he received the National Award of Applied Sciences and Technology from the Government of Chile. In 2015, he received the Eugene Mittelmann Award from the Industrial Electronics Society of the IEEE. From 2014 to 2020, he has been included in the list of Highly Cited Researchers published by Web of Science.